

Complete optical stack modeling for CMOS-based medical x-ray detectors

Alexander S. Zyazin*, Inge M. Peters

Teledyne DALSA Professional Imaging, High Tech Campus 27, 5656 AE Eindhoven,
The Netherlands

ABSTRACT

We have developed a simulation tool for modeling the performance of CMOS-based medical x-ray detectors, based on the Monte Carlo toolkit GEANT4. Following the Fujita-Lubberts-Swank approach recently reported by Star-Lack *et al.*, we calculate modulation transfer function $MTF(f)$, noise power spectrum $NPS(f)$ and detective quantum efficiency $DQE(f)$ curves. The complete optical stack is modeled, including scintillator, fiber optic plate (FOP), optical adhesive and CMOS image sensor. For critical parts of the stack, detailed models have been developed, taking into account their respective microstructure. This includes two different scintillator types: $Gd_2O_3:S:Tb$ (GOS) and $CsI:Tl$. The granular structure of the former is modeled using anisotropic Mie scattering. The columnar structure of the latter is introduced into calculations directly, using the parameterization capabilities of GEANT4. The underlying homogeneous CsI layer is also incorporated into the model as well as the optional reflective layer on top of the scintillator screen or the protective polymer top coat. The FOP is modeled as an array of hexagonal bundles of fibers. The simulated CMOS stack consists of layers of Si_3N_4 and SiO_2 on top of a silicon pixel array. The model is validated against measurements of various test detector structures, using different x-ray spectra (RQA5 and RQA-M2), showing good match between calculated and measured $MTF(f)$ and $DQE(f)$ curves.

Keywords: X-ray imaging, medical CMOS detectors, MTF, DQE, scintillator modeling, Monte Carlo, GEANT4

1. INTRODUCTION

Monte Carlo simulation is a powerful method widely used in numerous medical physics areas. In particular in diagnostic x-ray imaging this technique has been used to model in detail conversion layers, focusing among others on the granular^{1,2} and microcolumnar^{3,4} scintillators and even on scintillator optimization for specific clinical applications, taking into account anatomical tissue structure.⁵ However, to our knowledge, no work has been published, where the complete optical stack of the detector is modeled in detail and the effects of various detector components on the performance are studied.

As illustrated in Figure 1, modern indirect conversion medical x-ray detectors are complicated devices and the final image quality is determined by the multitude of the physical processes occurring in different parts of the detector from x-ray scattering and absorption in the top cover to electric charge generation in the pixels. The propagation of optical photons is central to the spatial resolution and noise performance of the detector, that are usually characterized by modulation transfer function $MTF(f)$, (normalized) noise power spectrum (N)NPS(f) and detective quantum efficiency $DQE(f)$ as function of the spatial frequency f . The purpose of this work is to develop and validate a Monte Carlo simulation tool where all the relevant processes throughout the complete optical stack are taken into account. Such a tool can be indispensable in understanding the performance and ultimately in designing new detector architectures.

*alexander.zyazin@teledynedalsa.com

Our simulation is implemented using open-source C++ GEANT4 toolkit and is experimentally validated on three test cases. The first one is a detector based on the well-documented Lanex Fast-back phosphor screen, the second one is a mammography-type detector with a thin (180 μm) microcolumnar CsI scintillator and the third case shows the application to a practical problem of defining optical adhesive thickness specifications for a general radiography detector.

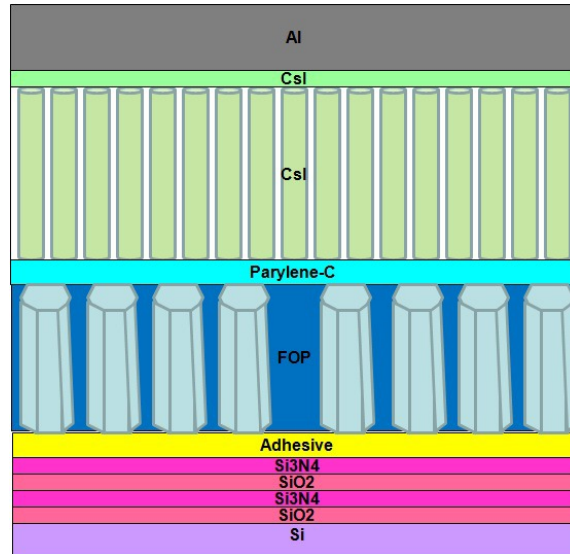


Figure 1. An optical stack example. A CsI:Tl scintillator (with a microcolumnar structure on top of a homogeneous layer, covered by a protective polymer, in this case Parylene-C) on aluminum foil substrate is flipped upside down and pressed on a fiber optic plate (FOP). The FOP is glued with optical adhesive to a CMOS sensor that has a few metallization layers. As discussed in the Methods section a thin air gap is normally introduced between the scintillator and the FOP when simulating this kind of “pressed on” geometries.

2. METHODS

2.1 Simulations

We follow the Fujita-Lubberts-Swank (FLS) approach recently proposed and described in detail by Star-Lack et al.^{6,7} Briefly, $MTF(f)$ is calculated using a simulated image of a tilted line. $NNPS(f)$ is calculated by performing a DFT on an ensemble of point spread functions (PSF) calculated from a collection of single x-ray event images. A total number of counts from each PSF is added to form a pulse-height spectrum (PHS). Swank factor A_s is computed from the statistical moments of the PHS. Quantum detection efficiency of the scintillator A_q is found straightforwardly as the ratio of the x-ray photons stopped by the scintillator to the total number of primary photons. The $DQE(f)$ curve can then be calculated as

$$DQE(f) = A_s A_q \frac{MTF(f)^2}{NNPS(f)}.$$

For shot-noise limited detectors the FLS algorithm as described above can generally yield MTF and DQE curves closely matching experimental data within short CPU time. However, three important considerations must be taken into account. First, within the FLS approach the detector is assumed to be perfectly linear. It does not model electronic readout noise, therefore it cannot predict performance variation with the x-ray dose. Second, the effect of direct x-ray hits that act as another source of spatially uncorrelated noise⁸ is not taken into account. Combined, these two noise sources might drastically degrade DQE performance at high spatial frequencies. Third, the simulations require a huge number of input parameters, describing geometry, physical properties and chemical composition of various detector components. Some of

these parameters are not known in advance, and can be challenging to characterize. A thorough validation of a model is therefore required, comparing the simulation results to experimental data obtained under various conditions (e.g., x-ray beam quality and dose), with as many controlled parameters as possible.

The readout noise value is determined solely by the pixel and readout circuit and does not depend on the optical stack configuration or the x-ray dose. Therefore, once known (e.g., from the measurements of a detector using the same readout circuitry at zero x-ray dose), it can be normalized by the $NPS(f=0)$ value and added to the simulated NPS. The effect of direct x-ray hits can be simulated by adapting the pixel model. However, that has not been implemented yet in our work. Instead we use an empirical correction procedure, based on the measurement data for NPS. The measured $NPS(f)$ curve is extrapolated to the zero frequency and the simulated $NPS(f)/NPS(0)$ curve is modified by adding $[NPS(f_N)/NPS(0)]_{meas} - [NPS(f_N)/NPS(0)]_{sim}$ value (where f_N is the Nyquist frequency) to the all data points, and that curve is renormalized to zero frequency afterwards. Results of this correction procedure are shown in Figure 2, illustrating original DQE overestimation. Note that this correction is only needed in the presence of a strong uncorrelated noise component in the measurement data, an example is discussed below.

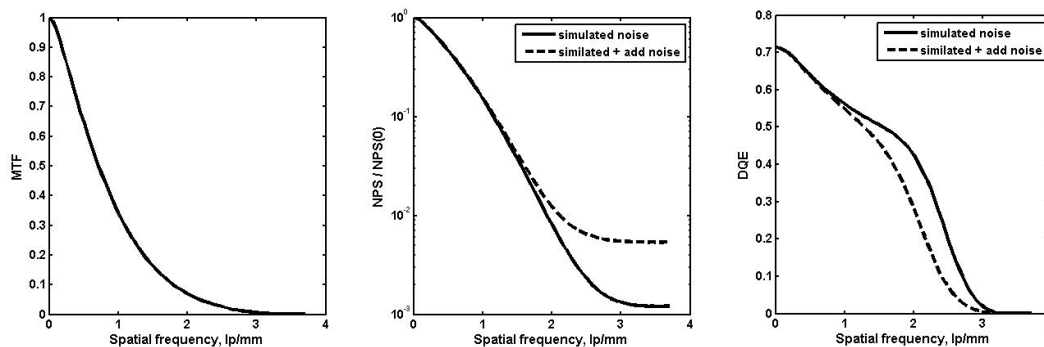


Figure 2. MTF, NPS and DQE curves illustrating correction for uncorrelated noise for a test detector with a pixel size of $135 \mu\text{m}$.

We implement our simulation tool using open-source C++ library GEANT4, version 10.0.2.⁹ This toolkit has been selected for several reasons. First, it combines both radiation and optical transport simulation within one package. Second, different pre-defined physical models can be selected to provide desired accuracy while keeping the computation time reasonable. Third, starting from version 10.0 it natively supports multithreaded mode, making efficient use of modern multi-core CPUs.

The detector is represented as a modular structure composed of several components: carbon cover, scintillator, fiber optic plate (FOP), optical adhesive and CMOS image sensor. These components in turn might consist of a few layers, e.g., the CsI scintillator might include a substrate foil, a uniform CsI layer, a layer of CsI pillars and a protective polymer top coat. Scintillator and FOP might have a microstructure that is critical for optical transport. Our tool is designed in such a way that it allows to include any layer and to change any relevant geometrical dimension, so that the effect of such changes on the detector performance can be easily traced.

Currently, simulations of two different scintillator types are supported. These are $\text{Gd}_2\text{O}_2\text{S:Tb}$ (GOS) and CsI:Tl. The GOS has a granular microstructure that is modeled using anisotropic Mie scattering approach.¹ The density of a GOS layer is adjusted to fit the fill factor. A pillar structure of CsI:Tl is modeled directly using parameterization capabilities of GEANT4. Cylindrical pillars with $6 \mu\text{m}$ diameter are placed in a hexagonal lattice arrangement such that the packing density is $\sim 85\%$. To check the impact of shape variation we have also modeled pillars as cuboids in a square lattice, retaining the same volume and packing density. We found that the MTF might slightly improve in this case, but the difference between the two arrangements does not exceed 2-3% (see for example Figure 4 in the discussion of a mammography-type detector). This, in fact, can be used to shorten the simulation time as the geometry setup stage is executed by GEANT4 $\sim 8-10$ times faster for the square lattice of cuboids compared to the hexagonal lattice of cylinders with the simulated detector dimensions typically used.

CsI microcolumns are typically grown on aluminum foils or on fiber optic plates. At the interface with the substrate a homogeneous CsI layer with typical thickness of several tens of micrometers⁴ is formed. It can be very challenging to

measure this thickness by traditional methods like scanning electron microscopy due to a few reasons. First, it is expected to have batch-to-batch variations even for nominally identical samples from the same vendor. Second, such a measurement is destructive by nature and the scintillator piece cannot be reused thereafter. Third, preparation for such a measurement can actually alter the morphology of the sample. Therefore, we use the thickness of homogeneous layer as a fitting parameter in our simulations. Note also that this thickness can vary substantially for different types of substrates (aluminum foil or FOP) due to differences in the thermalisation process during the crystal growth.¹⁰

The FOP is modeled as an array of hexagonal prisms (fiber bundles) with a 6 μm hexagon side embedded into a frame plate with increased absorption and smaller refractive index. Some of the fibers (typically 1 out of each 13) are removed leaving the frame plate material on their place to simulate black fibers that are used in order to increase spatial resolution of the FOP.

Table 1. Properties of selected materials used in the simulations. Optical parameters are given for the wavelengths range 340-720 nm. Values in parentheses refer to the wavelength of 540 nm.

Material	Density(g/cm ³)	Refraction index	Absorption length (cm)
CsI:Tl	4.51	1.771-1.906 (1.796)	1.0
Gd ₂ O ₂ S:Tb	3.27-5.57	1.7	4.0
FOP core material (G4_GLASS_LEAD)	6.22	1.77-1.90 (1.79)	1.32-123 (123)
FOP frame material (G4_GLASS_PLATE)	2.4	1.49	0.714-1.53 (1.53)
Parylene-C (C ₈ H ₉ Cl)	1.289	1.639	--
Optical adhesive (C ₂₁ H ₂₅ ClO ₅)	1.3	1.518-1.540	--
Carbon	2.0	1	0
Aluminum	2.699	1	0
PET (C ₁₀ H ₈ O ₄)	1.38	1.57	--
Cellulose acetate (C ₈ H ₁₃ O ₇)	1.44	1.5	--
Si ₃ N ₄	3.2	2.02-2.11 (2.035)	--
SiO ₂	2.32	1.46-1.48 (1.460)	--
Silicon	2.33	3.76-6.54 (4.053)	--

If the scintillator on aluminum foil substrate is pressed on the FOP and not coupled with an optical adhesive or oil, a thin (typically 1 μm) air gap is introduced to take that into account.¹¹

All the other layers above the CMOS sensor (carbon cover, optical adhesive, protective polymer, etc.) are simulated as homogeneous layers of the corresponding material. The relevant properties of these materials as used in the simulations are given in Table 1.

The CMOS sensor comprises a few metallization layers on top of a silicon substrate. The metallization layers are represented as silicon oxide/silicon nitride stacks with a known thickness. The silicon surface is divided into a pixel

array. For simplicity the pixels are modeled as a thin ($0.1 \mu\text{m}$) layer below the surface with a 100% fill factor. Each optical photon passing through a pixel volume is detected.

The x-ray source is modeled as a $50 \mu\text{m}$ wide line tilted by 5° with respect to the pixel orientation. When calculating presampling MTF we take into account the finite line width by dividing the MTF curve resulting from the FLS simulation by $\text{sinc}(0.05 * f)$, where f is the spatial frequency in lp/mm. We use tabulated values for RQA5 and RQA-M2 x-ray qualities as primary x-ray spectra.

Following previous authors,^{6,7} we found that in order to speed up the simulations the scintillation yield can be reduced compared to a real value without compromising MTF and DQE simulation results. We normally use a yield of 20,000 optical photons/MeV for CsI:Tl screens (instead of $\sim 50,000$ - $60,000$ photons/MeV), although even lower values in principle can be used. With this yield we typically run 5,000-10,000 primary x-ray events for a 200×200 pixels detector. We use the G4EmPenelopePhysics model provided by GEANT4 for low-energy electromagnetic physics together with an optical physics list with scintillation, boundary processes, optical absorption and Mie scattering (for GOS simulations) included. We found that the Rayleigh scattering of optical photons has negligible effect on the simulation results.

2.2 Measurements

The x-ray measurements were performed according to the IEC 62220-1 standard for the adhesive thickness experiments and GOS measurements using the RQA5 spectrum and the IEC 62220-1-2 standard for the mammography-type detector using the RQA-M2 spectrum. The MTF was measured using a sharply polished edge of a 1 mm piece of tungsten slanted by $\sim 5^\circ$. For the NNPS calculations 170 gain- and offset-corrected x-ray images were used for the adhesive thickness experiments and 35 images for the mammography-type detector. The measurements on the adhesive thickness were done on $5 \times 5 \text{ cm}^2$ samples while for the mammography detector a region of interest of 100 cm^2 was used as requested by the standard.

3. RESULTS

3.1 GOS scintillator

GOS phosphor screens are used in x-ray imaging already for a few decades and their properties are very well documented in the literature. They provide therefore an excellent platform to validate the simulation of other components. We model and characterize a detector based on a $300 \mu\text{m}$ thick Lanex Fast Back screen (Eastman Kodak Company, Inc.) pressed onto a 2 mm thick FOP that is glued with optical adhesive to a CMOS sensor with $100 \times 100 \mu\text{m}^2$ pixels. The adhesive thickness is used as a fitting parameter. To model the internal geometry of the screen we used data provided in a recent paper by Poludniowski and Evans.² Mie scattering parameters were calculated using our own routine, based on the $4.25 \mu\text{m}$ grain radius and packing fill factor of 0.6. We found Mie scattering length $l_{\text{Mie}} = 3.66 \mu\text{m}$ and an asymmetry factor $g = 0.80$. The GOS density is 4.46 g/cm^3 for this fill factor. Figure 3 shows the results of MTF and DQE simulation plotted together with the measurement data (RQA5 x-ray beam quality). The adhesive thickness of $20 \mu\text{m}$ is used in the simulation. We also add $1 \mu\text{m}$ air gap between the scintillator and the FOP as discussed in the Methods section. The results show a very good match at all spatial frequencies both for MTF(f) and DQE(f) curves and justify the use of the models for FOP, adhesive and CMOS sensor in further simulations of detectors with different, less well-documented scintillators.

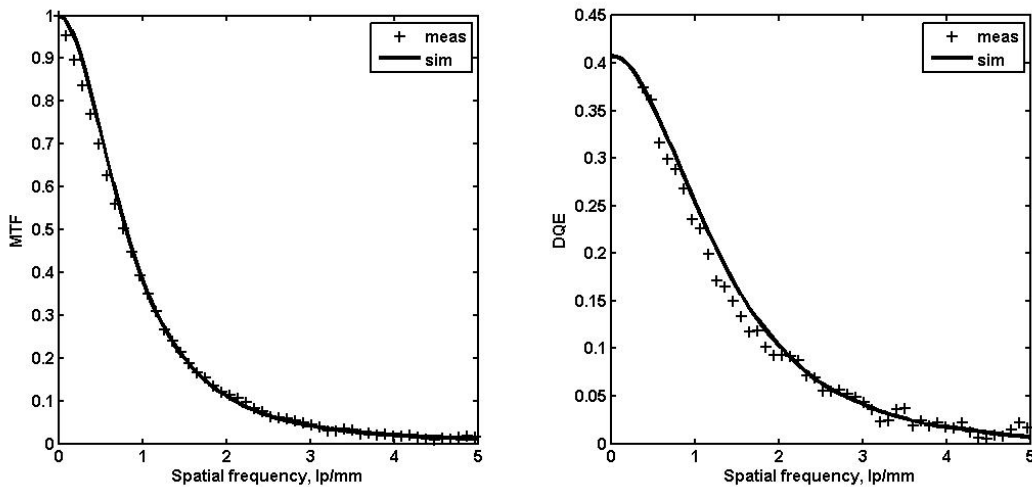


Figure 3. Experimental and simulated MTF and DQE curves for a Lanex Fast Back-based detector. The pixel size is $100\ \mu\text{m}$.

3.2 Mammography-type detector

For use in mammography applications scintillators thinner than in general radiography are required. Typical CsI:Tl thickness range for mammography is $150\text{-}300\ \mu\text{m}$ compared to $600\text{-}700\ \mu\text{m}$ for general radiography. Furthermore, different x-ray spectra are used. Therefore, optical stack simulations for mammography detectors should be validated separately. We have assembled a test detector based on a $50\ \mu\text{m}$ pixel CMOS sensor and performed a series of measurements using RQA-M2 spectrum. We use a high resolution $180\ \mu\text{m}$ thick CsI:Tl scintillator grown on a FOP. The scintillator plate is coupled to the sensor using optical oil. The detector is placed in a housing with a $1.5\ \text{mm}$ thick carbon top cover.

We have simulated this geometry, varying the oil thickness between 15 and $50\ \mu\text{m}$ and the homogeneous CsI layer thickness between 0 and $50\ \mu\text{m}$. We have also checked the impact of possible pillar shape variation by simulating pillars first as cylinders and then as cuboids with the same volume and fill factor. The results are presented in Figure 4. We have found that $30\ \mu\text{m}$ thick homogeneous layer and $150\ \mu\text{m}$ thick layer of cylindrical pillars in combination with $40\ \mu\text{m}$ thick oil yields the best match for the measured MTF data. We have observed however that the $\text{DQE}(f)$ curve is not reproduced well by the FLS routine (dashed lines in Figure 4). This results from an apparent underestimation of the simulated uncorrelated noise. The exact origin of this noise is yet to be found. It cannot be attributed to the readout noise of the detector, since the measurements were performed at high dose levels where this noise contribution is still negligible, also at higher spatial frequencies. Correction of the NPS curve as described in the Methods section, based on the experimental $\text{NPS}(f=10\ \text{lp/mm})$ value, yields for cylindrical pillars a matching $\text{DQE}(f)$ shape (blue solid line in Figure 4) albeit with a few percent lower absolute values. Note that the DQE values at high frequencies are reproduced better with a rectangular pillar cross section.

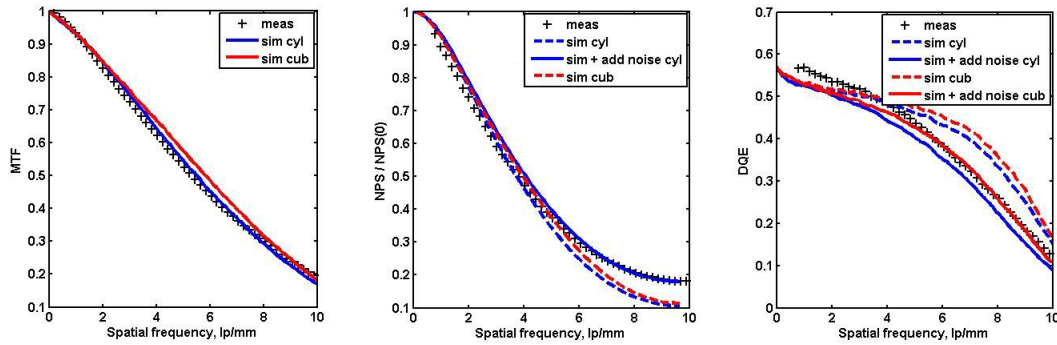


Figure 4. Experimental and simulated MTF, NPS and DQE curves for a 180 μm high-resolution CsI detector. The pixel size is 50 μm . The data are obtained using RQA-M2 x-ray beam quality.

3.3 Adhesive thickness

Control of the optical adhesive thickness between CMOS sensor and FOP or scintillator screen is an important practical problem faced by detector manufacturers. Too thick adhesive layer results in performance degradation due to light refraction. In large-area multi-tile devices the problem becomes even more challenging because of uneven silicon surface profile. Validated simulations can help to formulate appropriate specifications for the assembly process or even indicate means to improve optical stack tolerance to the thickness of the adhesive. On the other hand, experiments with a controlled thickness can themselves be an important validation tool for simulations.

To achieve a controlled thickness of the optical coupling medium, we have performed a series of measurements, using soda lime glass microspheres (Cospheric LLC, Santa Barbara, CA USA) of different sizes, ranging from 25 to 216 μm , dispersed in immersion oil (Cargille type 37, Cargille Laboratories, Cedar Grove, NJ USA). In these experiments we have used $5 \times 5 \text{ cm}^2$ 700 μm thick CsI:Tl grown on 2 mm thick FOP, coupled to a 100 μm pixel CMOS sensor. The sample area guarantees that large-scale flatness variations of the silicon surface are absent and the thickness of the optical oil layer, applied between the FOP and the sensor, is determined by the upper bound of the microspheres diameter distribution. Furthermore, we have repeated the measurements in different regions of the sensor and found that the results are reproduced as expected.

We have simulated this geometry, fixing the thickness of the oil and varying the thickness of the homogeneous CsI layer to match the measured MTF data. The best fit for all the adhesive thicknesses is obtained with the homogeneous layer with 150 μm thickness (and therefore 550 μm high columns). The protective polymer thickness is set at 15 μm . The results for four different adhesive thicknesses are shown in Figure 5. Both measured and calculated results for 25 μm and 75 μm are very close to the 50 μm data. They are not shown on the plots for the sake of clarity.

These results suggest that for this specific combination of pixel size, scintillator/FOP and the intended x-ray beam quality and dose, the assembly process specifications can be relaxed, allowing adhesive thickness as high as 100 μm .

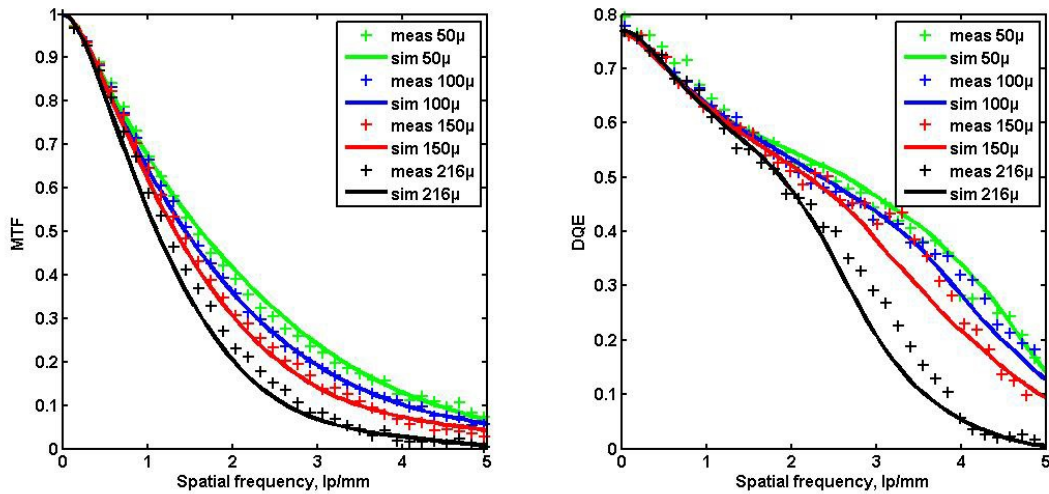


Figure 5. Experimental and simulated MTF and DQE curves for a detector based on a $700\ \mu\text{m}$ thick CsI-coated FOP coupled to a CMOS sensor using optical adhesive. The curves are measured and simulated for four adhesive thickness values between $50\ \mu\text{m}$ and $216\ \mu\text{m}$. The data are obtained using RQA5 x-ray beam quality. Detector pixel size is $100\ \mu\text{m}$.

For comparison we have simulated another detector arrangement with the same x-ray exposure conditions, pixel size and scintillator thickness, but without the FOP. Such a “FOP-less” architecture might be interesting for very low-dose applications because of increased light output and reduced costs. However, as can be seen from Figure 6, the MTF and especially DQE performance is rapidly degrading with the increasing adhesive thickness, requiring therefore stricter specifications. Note that in this case measurements with glass microspheres are challenging because the microspheres puncture the protective polymer layer, irreversibly damaging the scintillator.

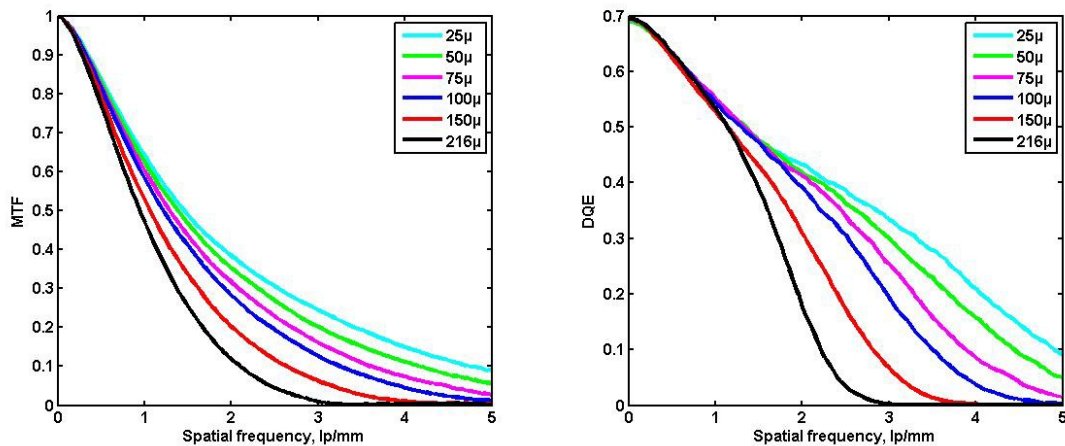


Figure 6. Simulated MTF and DQE curves for a $700\ \mu\text{m}$ CsI detector without FOP, directly coupled to a CMOS sensor. Curves of different colors correspond to different optical adhesive thickness. The pixel size is $100\ \mu\text{m}$. RQA5 x-ray beam quality.

4. DISCUSSION

Although a good match between the measurements and the simulations has been achieved for the reported three examples, the simulations still lack general predictive power. A few parameters are not well understood, in particular the thickness of the homogeneous CsI layer and its dependence on the total thickness or substrate type. In general, there is no

reason why the homogeneous layer should be thicker when the total thickness of the sample is increased. Nevertheless, our simulations (including simulations not reported here) clearly show that trend. The question may arise, if the 150 μm value resulting from the simulations of the 700 μm thick CsI on a FOP substrate is even realistic. In fact this parameter might be an effective measure of the light spread inside the CsI due to nonregular nature of the pillars and not the real geometric thickness of the interface layer. Further experiments and modeling are required to clarify this point.

Another step to improve the simulations is to introduce a pixel model that would take into account the quantum efficiency and would respond to the direct x-ray hits. Such a model would improve prediction of the high-frequency DQE. Since the direct hits count scales linearly with the dose, FLS algorithm with optimization measures like scintillation yield reduction can still be used, and this step will not lead to a significant increase of simulation time.

The simulations however proved very useful in understanding trade-offs of the optical stack, allowing to link general behavior and particular features of the MTF(f) and DQE(f) curve to the properties of single layers. This understanding is crucial for tailoring new detector designs for specific applications.

5. CONCLUSION

We have implemented the Monte Carlo simulation tool for modeling the x-ray transport and conversion, as well as propagation of optical photons in the medical CMOS x-ray detectors. The tool is validated by measurements in three different experimental settings with two different x-ray spectra. Application of the simulation to the practical problem of defining the adhesive thickness specification is demonstrated.

The authors would like to thank J. Miller for providing measurements data for the mammography detector and M. Koyuncu for assistance with the measurements of other detector types.

REFERENCES

- [1] Liaparinos, P. F., Kandarakis, I. S., Cavouras, D. A., Delis, H. B. and Panayiotakis, G. S., "Modeling granular phosphor screens by Monte Carlo methods," *Med. Phys.*, 33 (12), 4502-4514 (2006).
- [2] Poludniowski, G. G. and Evans, P. M., "Optical photon transport in powdered-phosphor scintillators. Part II. Calculation of single-scattering transport parameters," *Med. Phys.*, 40 (4), 04195 (2013).
- [3] Sharma, D. and Badano, A., "Validation of columnar CsI x-ray detector responses obtained with hybridMANTIS, a CPU-GPU Monte Carlo code for coupled x-ray, electron, and optical transport," *Med. Phys.* 40 (3), 031907 (2013).
- [4] Freed, M., Miller, S., Tang, K. and Badano, A., "Experimental validation of Monte Carlo (MANTIS) simulated x-ray response of columnar CsI scintillator screens," *Med. Phys.* 36 (11), 4944-4956 (2009).
- [5] Liaparinos, P. and Bliznakova, K., "Monte Carlo performance on the x-ray converter thickness in digital mammography using software breast models," *Med. Phys.* 39 (11), 6638-6651 (2012).
- [6] Abel, E., Sun, M., Constantin, D., Fahrig, R. and Star-Lack, J., "User-friendly, ultra-fast simulation of detector DQE(f)," *Proc. SPIE* 8868, 88683O (2013).
- [7] Star-Lack, J., Sun, M., Meyer, M., Morf, D., Constantin, D., Fahrig, R. and Abel, E., "Rapid Monte Carlo simulation of detector DQE(f)," *Med. Phys.* 41 (3), 031916 (2014).
- [8] Yun, S., Kim, H. K., Lim C. H., Cho M. K., Achterkirchen T. and Cunningham, I., "Signal and noise characteristics induced by unattenuated x rays from a scintillator in indirect-conversion CMOS photodiode array detectors," *IEEE Trans. Nucl. Sci.* 56 (3), 1121-1128 (2009).
- [9] Agostinelli, S. *et al.*, "GEANT4: A simulation toolkit," *Nucl. Instrum. Methods A* 506, 250-303 (2003).
- [10] Sabet, H., Prekas, G., Breen, M., Bhandari, H. B., Nickerson, P., Derderian, G., Robertson, F., Kudrolli, H., Cool, S. and Nagarkar, V. V., "High-performance and cost-effective detector using microcolumnar CsI:Tl and SiPM," *IEEE Trans. Nucl. Sci.* 59 (5), 1841-1849 (2012).
- [11] Yun, S. M., Cho, M. K., Lim C. H., Kim, H. K., Graeve, T., Cho, H. and Kim, J.-M., "Cascaded linear-systems analysis of CMOS flat-panel detectors for digital radiography," [Proceedings of the International Conference on Advanced Nondestructive Evaluation II], World Scientific Publishing, Busan, Korea, 804-809 (2007).